

# Unoccupied electronic states of Au(113): theory and experiment.

Patricio Häberle<sup>\*1</sup>, Wladimir Ibañez<sup>1</sup>, Rolando Esparza<sup>1</sup> and Patricio Vargas<sup>1,2</sup>

<sup>1</sup>*Departamento de Física, Universidad Técnica Federico Santa María, Casilla 110-V, Valparaíso, Chile*

<sup>2</sup>*Departamento de Física, Universidad de Santiago de Chile, P.O.Box 307, Santiago-2, Chile*

(versión 9.0, October 30, 2018)

We present results from Inverse photoemission spectroscopy in the isochromat mode, with angular resolution, from the clean Au(113) surface. To identify the origin of the different resonances we have performed first principles calculations of the bulk band structure in the LMTO formalism. Using the particular characteristic of the spectrometer we have made a theoretical prediction of the bulk features dispersion as a function of parallel momentum, considering only energy and momentum conservation. Thus we have been able to unambiguously identify, from measured spectra various bulk derived resonances in addition to two surface resonances and a surface state in the  $[\bar{1}10]$  and  $[3\bar{3}2]$  directions respectively.

\*email: phaberle@fis.utfsm.cl

PACS numbers: 73.20.-r, 73.20.At

## I. INTRODUCTION

The electronic structure of low index faces of noble metals has been the subject of many experimental studies using techniques such as photoemission, two photon photoemission and inverse photoemission. In particular several of those studies have dealt with the electronic structure above the Fermi level  $^{1-6}$  ( $\varepsilon_F$ ) of different noble metal surfaces. The main interest has been the description of image states and resonances together with the identification of crystal derived surface states<sup>7</sup>.

For Au(100), for example, there is data confirming the existence of a surface state within the band gap at  $\bar{\Gamma}$ <sup>8,9</sup> and also a surface resonance of a bulk derived features along the  $\bar{X}\bar{\Gamma}\bar{M}$  directions. Similarly Au(111) also shows a resonance which has been assigned to an image state in an energy region above the band gap at  $\bar{\Gamma}$ <sup>9,10</sup>. On Au(110)<sup>11</sup> there are two surface states at  $\bar{X}$  and one at  $\bar{Y}$  within a band gap, for energies above  $\varepsilon_F$ . For Au surfaces then, in every band gap at least one surface state has been detected; image states have been observed, even if the states are within the bulk allowed energy momentum region. All these surfaces have in common that they show a room temperature reconstruction, but little effect from it has been detected in the empty electronic states. The results presented below are no exception to this general rule.

Au is still a subject of interest as a fairly inert substrate to grow thin films of ferromagnetic materials<sup>12</sup> that display oscillatory magnetization. An important aspect, in these very thin films, is the mismatch between the lattice parameters of the substrate and the film. Both the morphology of the growth and therefore the physical properties of the films are strongly dependent on this parameter. In the search for the proper growth orientation and mass density of the epitaxial layers, vicinal surfaces as fcc(113) could be considered, but there is a lack of both experimental and theoretical description of their electronic structure. In the case of thin films<sup>13,14</sup>

both the width and intensity of the unoccupied adsorbate induced resonances have been shown to depend on the details of the substrate electronic structure.

In the present study we describe the unoccupied electronic states of Au(113) along the two principal axis of this surface. We used Inverse photoemission spectroscopy (IPS) together with first principle calculations of the bulk band structure to provide a complete interpretation of the origin and nature of the different resonances present in our measurements. Using numerical calculations to describe the bulk band structure and its projection on a particular direction we have been able to label the different surface resonances and states, independent of the complexity of the measured surface electronic structure. This numerical-experimental combination should prove valuable in the description of the unoccupied states of thin metallic layers.

## II. EXPERIMENTAL

Inverse photoemission spectroscopy (IPS) is a technique which renders information regarding the unoccupied band structure of a solid<sup>15</sup>. The usual energy range considered goes from  $\varepsilon_F$  up to 10 or 15 eV above, including specially the energy region below the vacuum level. Our experiments were performed in a vacuum chamber equipped with an isochromat inverse photoemission spectrometer, based on a design by Dose<sup>16</sup>. The photon detector is a Geiger Müller counter filled with Iodine as a discharge gas and He as a buffer gas. The window that accepts the photons into the detector is a polished  $SrF_2$  disc. The combination of the bandgap of the window and the ionization potential of Iodine makes this detector highly sensitive to photons in a very narrow band around  $(9.5 \pm 0.3)$  eV<sup>4</sup>. The electron beam is produced by an electron gun based on a design by Zipf<sup>17</sup>. It

consists of a BaO cathode indirectly heated by a tungsten filament, an electron extraction element and a focusing lens. The measured energy resolution at 10 eV is 0.4 eV (FWHM) as measured by detecting the current on a flat metallic sample, subject to a ramp of increasing repulsive potential. The sample is mounted on a goniometer with both an azimuthal rotation and a rotation through an angle  $\theta$  around an axis on the plane of the sample. This is an improved manipulator which allows a much more precise and reproducible positioning than the one we used on a preliminary measurement on this same system<sup>18</sup>. The azimuthal angle is adjusted such that the electron momentum parallel to the surface ( $\hbar k_{//}$ ) is oriented along some major crystallographic direction. By changing  $\theta$  we can change the angle between the surface normal and the incident electronic momentum ( $k$ ). Both the power supply which controls the electron gun and the counter attached to the detector are connected to a personal computer via an interface using the GPIB protocol. A typical spectrum shows the photon intensity as a function of the energy of the incoming electrons in increments of 0.2 eV. The onset of the counts determines the location of ( $\varepsilon_F$ ). A resonance in one of these spectrum can be represented as a point in a energy-momentum ( $\varepsilon$  vs.  $k_{//}$ ) plane using the relation  $k_{//} = \sin\theta \sqrt{\frac{2m}{\hbar^2}(\varepsilon + \hbar\omega - \phi)}$ , with  $m$  being the electron rest mass,  $\varepsilon$  the energy of the resonance measured with respect to ( $\varepsilon_F$ ),  $\hbar\omega$  the energy of the detected photons,  $\phi$  the work function of the sample and  $\theta$  has been defined above.

The sample was prepared from 5N Au boule which was first mechanically polished and then electropolished with the surface normal oriented within a  $0.5^\circ$  of the  $[113]$  direction as verified by x-ray diffraction. It was successively sputtered with 1 keV  $Ar^+$  ion beam and annealed to  $450^\circ\text{C}$ . The surface displays a Low Energy Diffraction (LEED) pattern consistent with a clean surface. It shows a reconstruction close to a  $(1 \times 5)$  symmetry.<sup>19,20</sup> A previous study of this surface using x-ray diffraction<sup>21</sup> have shown this reconstruction to be incommensurate with the substrate, but no structural model for the surface has yet been proposed. From the LEED pattern itself we can not determine if the phase is incommensurate unless a detailed LEED I-V or other structural study is carried out.

### III. NUMERICAL CALCULATION

In order to determine the origin of the electronic resonances that appear in our measurements. We performed a detailed calculation of the pure bulk states of Au in the fcc structure at the equilibrium lattice parameter.

The calculation of the electronic structure of bulk Au was performed using standard LMTO techniques<sup>22</sup>, with a lattice parameter  $a = 4.08\text{\AA}$ , in the fcc structure. A

mesh of 18 points along each of the three primitive reciprocal translation vectors and the tetrahedron method was used to perform integrations in the Brillouin zone.

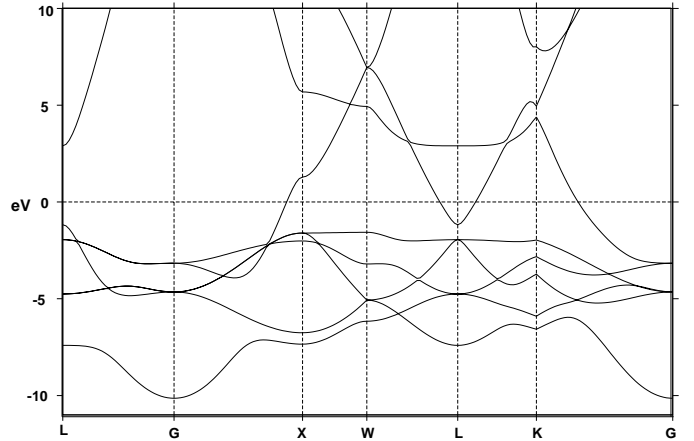


FIG. 1. Dispersion of the energy bands of Au along main crystallographic directions as calculated in the LMTO formalism

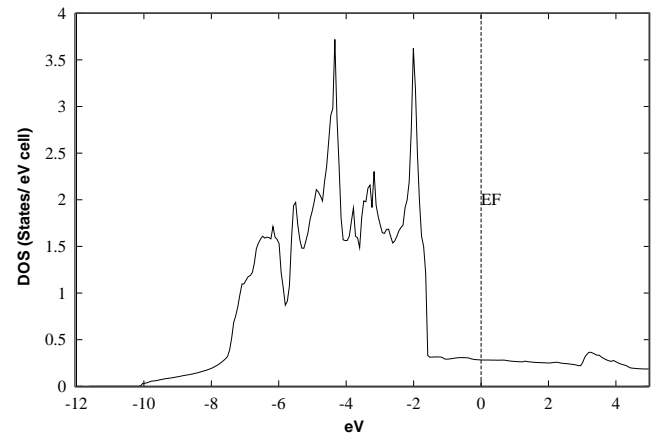


FIG. 2. The corresponding density of states for the bands described in the previous figure. The zero in the energy axis is fixed at ( $\varepsilon_F$ ). The wide peak centered at -4.5 eV corresponds to the d-band. The states above ( $\varepsilon_F$ ) have a dominant s-p character.

Figure 1 shows the result of our calculation for the standard band structure in different directions along the principal axis of the Brillouin zone. We can also determine the total density of states (DOS) as a function of energy (Figure 2) which could be compared to previous calculations. In order to help us in the interpretation of our experimental IPS measurements, we have performed a projection of the electronic states along the two main perpendicular directions of the  $(113)$  surface, namely  $[\bar{1}10]$  and  $[33\bar{2}]$  directions. This operation is simply to repre-

sent in a single graph all the energy states with a common  $k_{//}$ , regardless of the momentum in the direction normal to the surface. Figures 4 and 5 show the projected bands along the two perpendicular directions (in units of  $\text{\AA}^{-1}$ ) referred to the Fermi energy (in eV). The density of points in the graph reminds us of the underlying symmetry of the projected states which can be visualized because for both figures we have used a mesh of 100 points for the complete range of  $k_{\perp}$ . It is easy to recognize the existence of energy gaps between 1 eV and 3 eV above the Fermi energy in both directions. These gaps can be labeled with a combination of X and L character, with  $k_X = (1, 0, 0)$  and  $k_L = (\frac{1}{2}, \frac{1}{2}, \frac{1}{2})$  in units of  $2\pi/a$ .

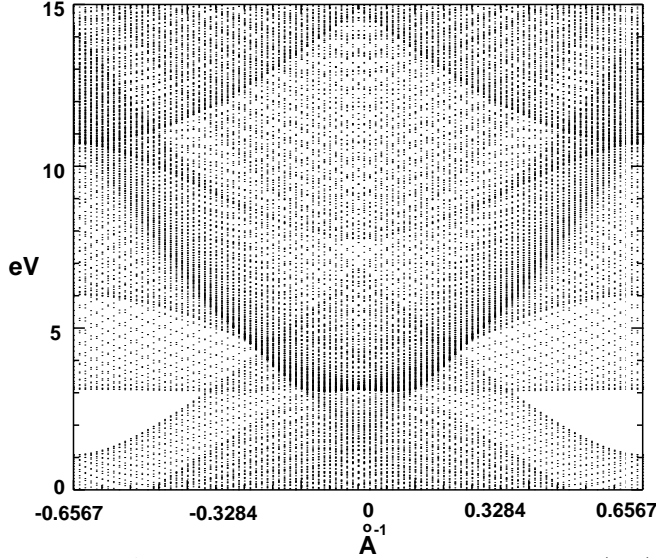


FIG. 3. Au fcc bulk band structure projected in the (113) surface along the  $[33\bar{2}]$  direction in  $k$  space. The energy scale are referred to  $(\varepsilon_F)$ . The  $k$  axis is in  $\text{\AA}^{-1}$  ( $a = 4.08 \text{\AA}$ ). At the extreme of the SBZ we can see an energy band gap between 1eV and 3eV, which becomes narrower for small  $k_{//}$  until it disappears at  $k_{//} \approx 0.33\text{\AA}^{-1}$ .

To further visualize the location these energy gaps we calculated all the electronic states on the unitary cube of side  $(4\pi/a)$  in the reciprocal space. Figure 5 shows a constant energy surface of the electronic states between 2.5 eV and 3 eV above  $\varepsilon_F$  in this unitary cube. This small energy range is chosen to provide enough points for a suitable representation of the surface, as required by the smoothing and fitting routines used to generate the graph. The cube has been rotated in such a way that the  $[113]$  direction comes out normal to the plane of the figure.

This constant energy surface shows two sets of gaps. Each one of them located symmetrically, along the two main perpendicular axis, and also to the projection of the origin of the inverse space onto the (113) plane ( $\bar{\Gamma}$ ).

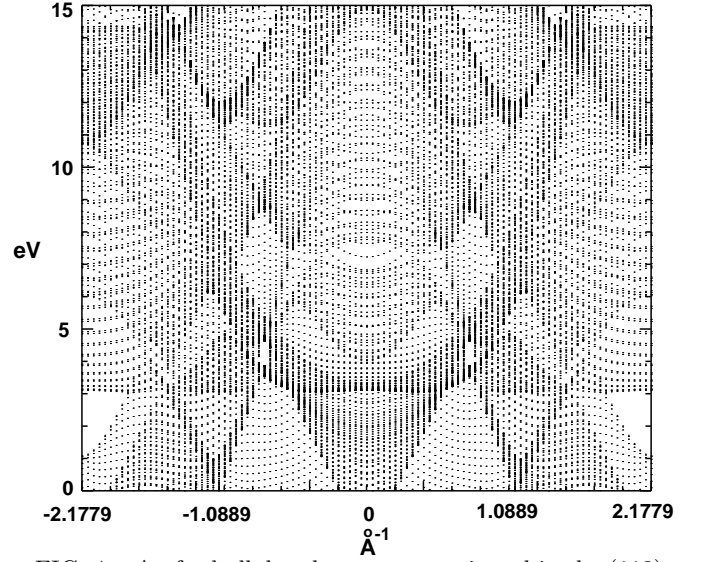


FIG. 4. Au fcc bulk band structure projected in the (113) surface along the  $[\bar{1}10]$  direction. The energy scale are referred to  $(\varepsilon_F)$ . The same band gap observed in the previous figure can also be reached along this direction.

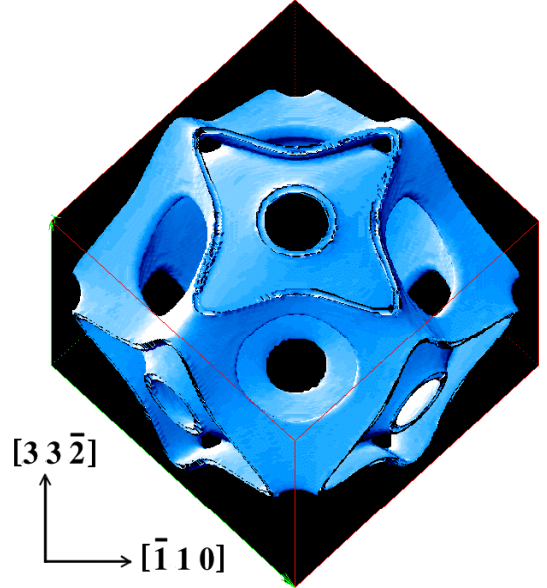


FIG. 5.  $k$ -space surface of constant energy (2.5  $\rightarrow$  3.0)eV above  $(\varepsilon_F)$  for Au electronic bulk states. The  $[113]$  direction in the reciprocal lattice is normal to the plane of the figure.  $\bar{\Gamma}$ , the projection of origin in  $k$ -space is at the symmetry center of the constant energy surface. Two set of band gaps are clearly seen for the main perpendicular directions. Only one of them retain this character (along the  $[33\bar{2}]$  direction) after the electronic states are projected onto the surface.

In an extended representation of the inverse space only the gaps shown along the  $[33\bar{2}]$  direction remains. The

rest of the space is filled by the electronic states from other zones with their respective centers slightly displaced. In particular the gaps along the  $[\bar{1}10]$  direction disappear and they can not be observed in the surface projected band structure (see Figure 4).

The two gaps, located symmetrically with respect to  $\bar{\Gamma}$ , along the  $[33\bar{2}]$ , could also be seen along the perpendicular direction as shown Figures 3 and 4, simply because of the peculiar shape of surface Brillouin zone for the (113) surface (see Figure 6).

By inspection of Figure 5 we can clearly see that the gaps in this energy region occurs by the exact superposition in k-space of the projections of the necks joining the neighboring cubes along the six  $[100]$  equivalent directions and the gaps in the zone boundary along the cube diagonals ( $[111]$  direction). In the next section we will see how this information is relevant in the labeling of the different surface resonances as seen by IPS.

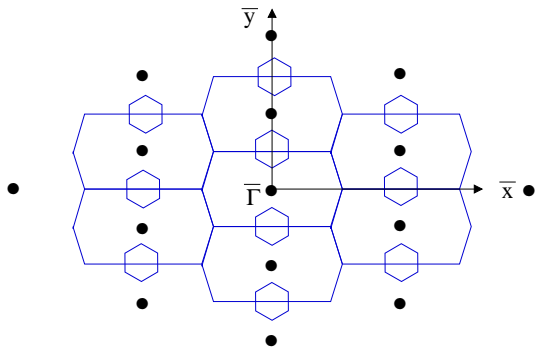


FIG. 6. Representation of the SBZ for the (1x1) fcc(113) surface. The dots are the projection of the reciprocal space in the (113) plane.  $\bar{x}$  and  $\bar{y}$  are  $[\bar{1}10]$  and  $[33\bar{2}]$  directions respectively. The hexagons represent the location of the energy gaps above the Fermi level in k-space. Starting from  $\bar{\Gamma}$  and going along  $\bar{x}$  there is an energy gap beyond the SBZ boundary. This same gap can also be reached along the  $\bar{\Gamma} - \bar{y}$  direction. The projected electronic structure of figures 3 and 4 show the actual extent of this gap in each direction .

## IV. EXPERIMENTAL RESULTS AND DISCUSSION

### A. $[\bar{1}10]$ direction

We will consider first a set of spectra along the the direction of the close packed rows ( $[\bar{1}10]$ ). Since the reconstruction of the surface shows no change in the surface periodicity along this direction, as judged from the LEED diagrams, one should not expect a large influence of the atomic rearrangement on the surface electronic structure. Figure 7 shows a series of IPS spectra for different angles of the incoming electrons respect to the surface normal. The Fermi level is clearly distinguishable as the onset for

the photon intensity and it has been used as the origin for the energy scale. The intensity is measured as photons/(electrons  $\times$  energy) but they are presented in an arbitrary scale. Some of the spectra have been re-scaled to facilitate their display.

There are clearly two sets of resonances, one them located above 10 eV from  $\varepsilon_F$  and the other one below 5 eV. The high energy resonances are fairly weak in intensity and show very little dispersion in energy. The low energy resonances instead are fairly well defined, which makes easier the identification of their evolution as the angle respect to the surface normal is changed. Also these states disperse over a wider energy range as can be seen directly from Figure 7.

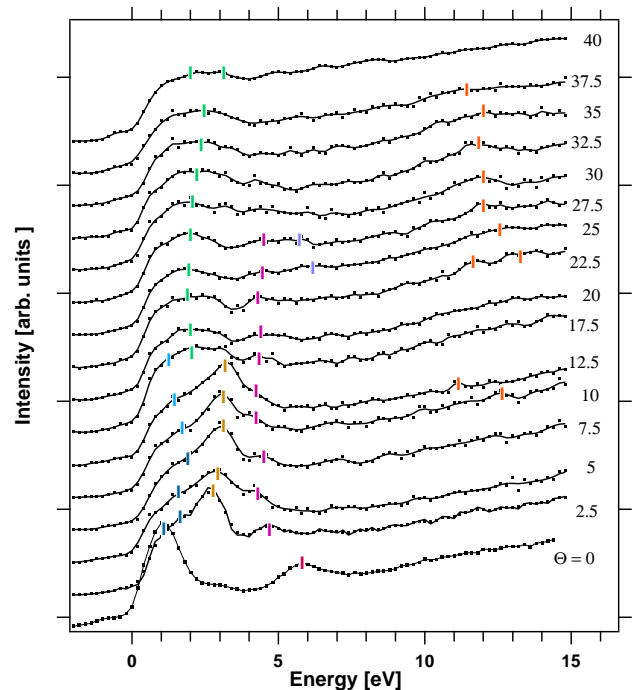


FIG. 7. Superposition of a set of IPS spectra. They display the photon intensity as a function of the energy of the incoming electrons. The square data markers correspond to the actual reading of each energy channel. The thin line is a smoothed spline to guide the eyes through the data. Several surface resonances have been highlighted with vertical lines

In Figure 8 we show a plot of the  $\varepsilon$  vs.  $k_{//}$  plane for this particular azimuth, with the parallel momentum along the  $[\bar{1}10]$  direction. The filled squares are the result of the numerical calculation. They represent the energy and momentum of a final state for a transition from an energy state  $9.5 \pm 0.3$  eV higher but for the same value of  $k$ . The calculated points are derived from the bulk energy bands calculated as described in the previous section. This way of finding the transitions is a more realistic than using the parabolic approximation to map the energy dispersion of a particular surface state or resonance. The choice of the energy difference is done to match the IPS's detector response. In this way, the square points correspond

to a theoretical prediction of bulk derived features of an IP experiment, based on a first principle calculation of the solid energy bands. It should be also noted that the energy difference between final and initial state is not exactly 9.5 eV, we have added a 0.3 eV Gaussian noise to mimic the experimental response. This calculation does not include the spectral weight associated with the matrix element effects on the optical transitions, which can drive some of the predicted events below the detectability limit.

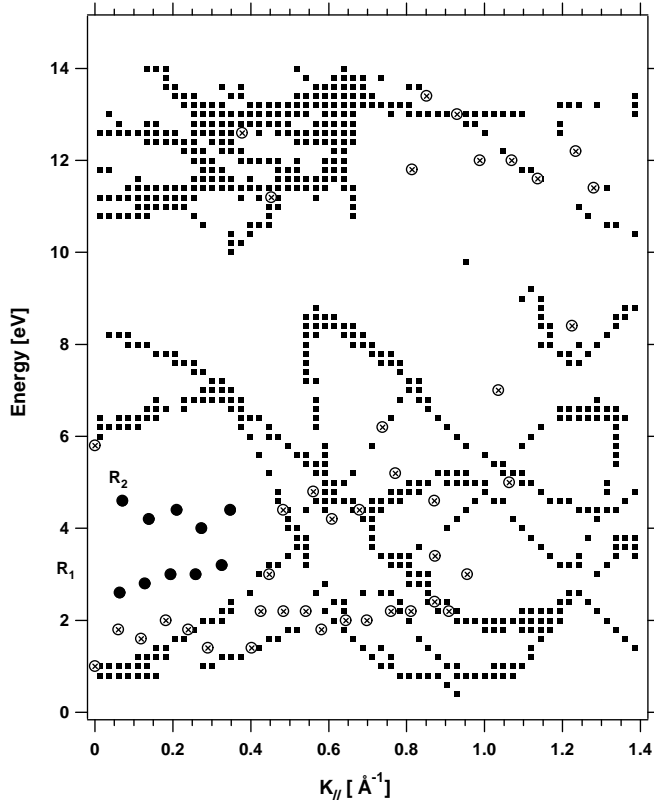


FIG. 8. Dispersion of the surface resonances as a function of  $k_{//}$ . The experimental data is shown by the circles( $\oplus$  and  $\bullet$ ). The theoretical prediction for bulk derived transitions are labeled by the filled squares.  $R_1$  and  $R_2$  are surface resonances. See text for further details.

The circular data markers in Figure 8, come from the measured data (Figure 7) and they correspond to the different resonances in each spectrum. We have chosen to separate them in two groups, one of them, all data points that superpose with calculated values of bulk derived features( $\oplus$ ) and the other set are those clearly located in a gap( $\bullet$ ) for the allowed bulk transitions. It should be clear that there is no absolute gap along this azimuth, the voids in the  $\varepsilon - k$  plane, shown in Figure 8 are related to the restrictions on energy and momentum imposed on the bulk transitions. We can then associate several resonances to bulk derived features, but at the same time we can recognize the existence of surface resonances, ( $R_1$

and  $R_2$ ) since they show no superposition with the calculated transitions.  $R_1$  behaves as a typical image state, since the energy is a minimum at low  $k_{//}$  values and then it increases for larger  $k$ . Rigorously it can not be labeled as an image state since it does not happen in a gap of the bulk energy bands. The second resonance  $R_2$  at about 4.4 eV above  $\varepsilon_F$ , just below the vacuum level, could then be interpreted as the higher energy states of the Rydberg series of image states. It is indeed surprising that these transitions are intense enough to be detected since there is no absolute gap in the bulk states for this energy region, hence the associated wave function should not be well localized at the surface. The argument in favor for this interpretation in the case of  $R_2$ , is the almost flat dispersion with  $k_{//}$  the resonance, which keeps it confined by the image potential below the vacuum level.

### B. [332] azimuth

As in the perpendicular direction (Fig. 7) in Figure 9 we show a complete set IPS spectra, where we can clearly identify several resonances with large dispersions, spanning in some cases an energy range as large as 2 eV.

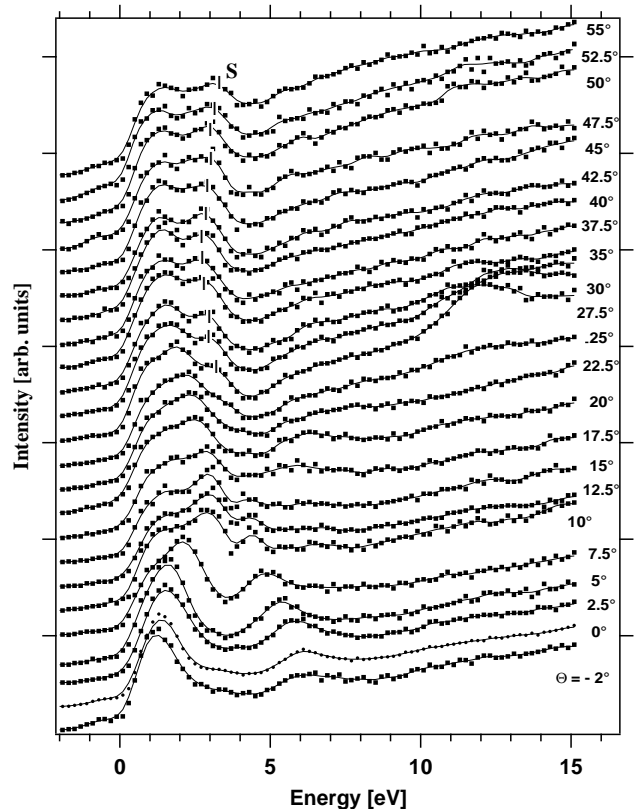


FIG. 9. IPS spectra along the [332] direction. Measured data points are the solid squares. The resonance labeled by  $S$  is a surface state.

At low angle we have two prominent resonances in the spectra. One of them which at normal incidence starts dispersing towards the Fermi level from about 6 eV, down to 4 eV at about 15° off normal. Another prominent resonance starts from 1.3 eV above the Fermi level at normal incidence increasing its energy up to 2.9 eV at about 17.5°. At 30° a new resonance emerges ( $SS$ ) at about 3 eV and as the angle increases it moves towards the Fermi level arriving at a minimum energy at about 40°. For larger angles it moves back to higher energies and can it be clearly detected as far as 55° off normal.

We have represented all these resonances in a  $\epsilon$  vs.  $k$  plane in Figure 10. The dark circular markers are the data points taken from the IPS spectra and the black squares are again the theoretical prediction for the bulk allowed transition. In addition we have encircled in a solid line the region of the absolute energy gap for this azimuth as determined from our calculation shown in Figure 4. Most of the experimental data points are on top of the bulk allowed transition and follow closely the dispersion of the calculated features. Exception to this statement is the state labeled  $S$ , which is clearly contained in the absolute energy gap, so we can label it legitimately as a surface state. The differences between the nature of  $S$  and the resonances along the  $[\bar{1}10]$  direction,  $R_1$  and  $R_2$ , are subtle but clear.  $R_1$  is contained in a "spectrometer energy gap", while  $S$  is within an absolute band gap. In addition  $R_1$  shows a typical upwards dispersion as  $k_{//}$  increases. This behavior could be associated with a free particle wave function dispersion not necessarily derived from the crystalline energy bands.

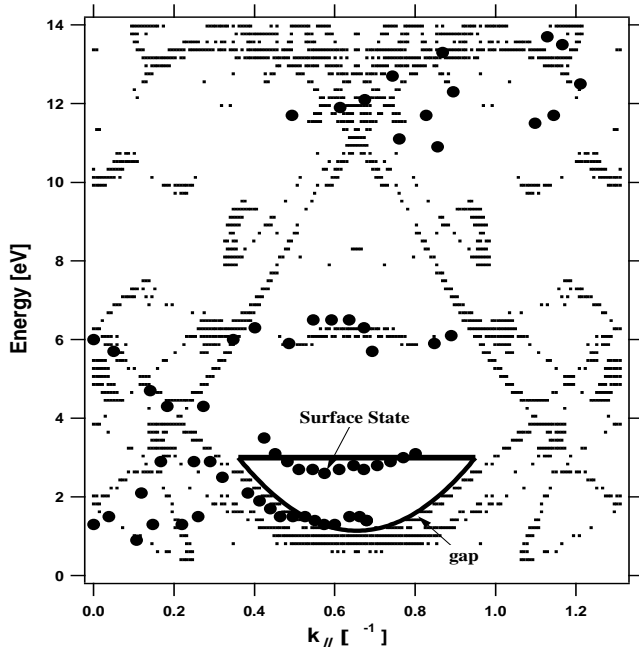


FIG. 10. Experimental resonances (•) and bulk predicted transitions (black squares). The surface state is clearly contained in the gap.

In fact this is in contrast with the dispersion of  $S$  which clearly follows the symmetry of the nearby energy bands, distinguishing it from an image charge type states which has its minimum energy at ( $\Gamma$ ). The surface state  $S$  has its minimum energy at the zone boundary ( $k_{//} = 0.66 \text{ \AA}^{-1}$ ).

## V. CONCLUSIONS

We have studied using IPS the empty electronic states of Au(113) from the Fermi level up to 15 eV along the two main crystallographic axis:  $[\bar{1}10]$  and  $[33\bar{2}]$ . In addition we calculated from first principles the Au band structure. We used this information to perform a surface projection of the bulk electronic structure and determine the locations of the surface energy gaps. Comparing the experimental results with the transitions predicted by our calculation we were able to recognize several surface resonances. Some of them were derived from bulk states. From the calculations we gained insight on the nature and origin of two surface resonances (along  $[\bar{1}10]$  direction with energies 4.3 eV and 2.7 eV near normal incidence) and a surface state (along  $[33\bar{2}]$ , with a minimum energy of 2.7 eV at  $k_{//} \approx 0.6 \text{ \AA}^{-1}$ ). Undoubtedly our experimental results in conjunction with the theoretical analysis presented here shows that isochromat IPS is a fairly powerful technique to study the unoccupied energy bands of single crystalline structures.

## ACKNOWLEDGMENT

We give special thanks to Dr. Dave Zehner for his help in preparing the crystal. This research received financial support from FONDECYT grants # 1990812 and 1990304, Fundación Andes grant C-10810/2 and ICM P99-135-F.

## REFERENCES

- <sup>1</sup> D.P. Woodruff, N. V. Smith, P. D. Johnson and W. A. Roger, Phys. Rev. B **26**, 2943 (1982).
- <sup>2</sup> B. Reihl, K. H. Frank, R. R. Schlittler, Phys. Rev. Lett. **52**, 1826 (1984).
- <sup>3</sup> R. A. Bartinsky, T. Gustafsson and P. Soven, Phys. Rev. B **31**, 4745 (1985).
- <sup>4</sup> A. Goldman, V. Dose, G. Borstel, Phys. Rev. B **32**, 1971 (1985).
- <sup>5</sup> N. V. Smith, Phys. Rev. B **32**, 3549 (1985).
- <sup>6</sup> C. T. Chen and N. V. Smith, Phys. Rev. B **40**, 7487 (1989).

- <sup>7</sup> Unoccupied Electronic States, eds J.C. Fuggle and J. E. Inglesfield (Springer-Verlag, Berlin, 1992).
- <sup>8</sup> F. Ciccacci, S. De Rossi, A. Taglia and S. Crampin, J. Phys. Conds. Matter **6**, 7227 (1994).
- <sup>9</sup> D. Straub and F. J. Himpsel, Phys. Rev. Lett. **52**, 1922 (1984).
- <sup>10</sup> D. P. Woodruff, W. A. Roger and N. V. Smith, Phys. Rev. B **34**, 764 (1986).
- <sup>11</sup> R. A. Bartinsky and T. Gustafsson, Phys. Rev. B **33**, 6588 (1986).
- <sup>12</sup> F. J. Himpsel, Phys. Rev. B **44**, 5966 (1991).
- <sup>13</sup> S. Crampin, S de Rossi and F. Ciccacci, Phys. Rev. B **53**, 13817 (1996).
- <sup>14</sup> D. Arena, F. Curti, R. Bartynski, Phys. Rev. B **56**, 15404 (1997).
- <sup>15</sup> J. B. Pendry, J. of Phys C **14**, 1381 (1981).
- <sup>16</sup> G. Denninger, V. Dose, H. Scheidt, Appl. Phys. **18**, 375 (1979).
- <sup>17</sup> P. Erdman and E. Zipf, Rev. Sci. Instrum. **53**, 225 (1982).
- <sup>18</sup> P. Häberle, Phys. Low-Dim. Struct. **10/11**, 317 (1995).
- <sup>19</sup> M. Sotto and J. C. Boulliuard, Surf. Sci. **214**, 97 (1989).
- <sup>20</sup> Q. T. Jiang, T. Gustafsson, P. Häberle and D. M. Zehner, Phys. Rev. B **45**, 14256 (1992).
- <sup>21</sup> A. Sandy, X-Ray scattering studies of metal surfaces, Ph. D. Thesis, (MIT, Boston, 1992).
- <sup>22</sup> O.K. Andersen and O. Jepsen, Phys. Rev. Lett. **53**, 2551 (1984). O.K. Andersen, O. Jepsen, and D. Gloetzel in Highlights of Condensed Matter Theory, eds. F. Bassani, F. Fumi, and M.P. Tosi (North-Holland, New York 1985) O.K. Andersen, O. Jepsen and M. Sob, in Lecture Notes in Physics: Electronic Band Structure and Its Applications, eds. M. Yussouff (Springer-Verlag, Berlin, 1987).